Phase equilibria and mineral parageneses of metabasites in low-grade metamorphism

J. G. LIOU, S. MARUYAMA, AND M. CHO

Department of Geology, Stanford University, Stanford, California 94305, USA

ABSTRACT. The system Na_2O–CaO–MgO–Al_2O_3–SiO_2–H_2O is proposed to model phase equilibria and mineral parageneses for low-temperature metamorphism of basaltic rocks. Univariant reactions marking the transitions between various sub-greenschist facies are identified and some have been experimentally determined. The introduction of Fe_2O_3 into the model system at fixed FeO/MgO ratio creates continuous reactions for facies boundaries and discontinuous reactions for invariant points of the model system. Both qualitative and quantitative effects on P–T displacement and phase compositions are discussed. The $X_{Fe^{3+}}$ isopleths for epidote were plotted to exemplify the transition from the zeolite through prehnite–pumpellyite to prehnite–actinolite facies. T–$X_{Fe^{3+}}$ relations were established for continuous and discontinuous reactions relating such facies transitions. Because of the common occurrence of two or three Ca–Al hydrosilicates in low-grade metabasites, an isobaric Al–Ca–Fe^{3+} projection from chlorite may be used to illustrate mineral assemblages and compositions of the coexisting Ca–Al silicates in the presence of quartz, albite, and chlorite. Reported occurrences in several classic burial metamorphic terrains and ocean-floor metabasites in ophiolites are described. Only the composition of a mineral from a buffered assemblage can constrain the intensive properties for metamorphism; previously reported compositional trends for pumpellyite and epidote with increasing metamorphic grade are oversimplified.

KEYWORDS: metamorphism, metabasites, sub-greenschist facies, zeolites, prehnite, pumpellyite, actinolite, epidote.

VERY low-grade metamorphism and hydrothermal alteration of basaltic rocks are universal processes; such processes have been increasingly recognized through detailed investigations of lithologies from both divergent and convergent lithospheric plate boundaries. Major portions of the oceanic crust appear to have been subjected to mid-oceanic, hydrothermal metamorphism immediately after their creation at a spreading ridge. When transported to the continental margin, the oceanic mafic rocks are again recrystallized at or near convergent plate junctions; the alteration and deformation trends depend on whether the oceanic

crust participated in a collision with the continent or was subducted or overridden by a continental plate. The processes of low-grade metamorphism of basaltic crust, therefore, are a function of tectonic setting. Each setting has its own appropriate thermal gradients, fluid compositions and many other intensive parameters and hence metabasalt displays characteristic mineral parageneses and compositions.

In spite of extensive investigation of low-grade metabasites over the last two decades, characterization of phase relations and mineral compositions in these rocks is not adequate due to the lack of an appropriate model system for basaltic assemblages. In the present study, the NCMASH (Na_2O–CaO–MgO–Al_2O_3–SiO_2–H_2O) system was selected to model parageneses and phase equilibria in low-grade metabasites. A petrogenetic grid for the model system was constructed, and several key reactions defining the facies boundaries were experimentally determined. The effects of FeO and Fe_2O_3 on compositions and phase relations in the model NCMASH system were then considered using the principle of sliding equilibria and available compositions of natural Ca–Al silicates from classical regions. T–$X_{Fe^{3+}}$ relations were established for parageneses in the zeolite, prehnite–pumpellyite, pumpellyite–actinolite, and prehnite–actinolite facies as defined in this paper (see later section for discussion). It is hoped that geologists who attempt to reconstruct the tectonic–metamorphic history can apply this petrogenetic grid to obtain quantitative information regarding temperature, pressure, and tectonic-chemical environments of recrystallization of metabasaltic rocks.

However, application of the petrogenetic grid to natural systems is not without difficulty. Obvious problems include complex bulk compositions, mixed component volatiles, metasomatism, slow kinetics, and redox reactions involved in natural low-grade metamorphic reactions. Moreover, most of the low-grade metamorphic minerals are solid

solutions and the appearance and disappearance of some index minerals (e.g. prehnite, pumpellyite, and epidote) is controlled by many continuous reactions. Examples of such continuous reactions have been recently described (e.g. epidote-pumpellyite by Nakajima et al., 1977; prehnite-epidote by Liou et al., 1983). Using this principle, chemographic relations of mineral assemblages and compositions for low-, intermediate-, and high-pressure facies series are presented.

Model basaltic system

The system $Na_2O-CaO-MgO-Al_2O_3-SiO_2$, commonly known as NCMAS, has long been recognized as one of the most important simple systems for modelling solid-liquid phase relations involved in the formation and crystallization of basaltic magma (Bowen, 1928). If M is equated with $MgO + FeO$, then NCMAS makes up more than 95% by weight of most basaltic rocks and most experimental studies of the genesis of basaltic liquids have been confined to this system. Therefore many supersolidus petrogenetic grids for the NCMAS system have been proposed (e.g. Bowen, 1928; Presnall et al., 1979) in order to obtain a better understanding of the origin and differentiation of basaltic magmas.

Similar justification can be applied to the treatment of low-grade metabasites which have been recrystallized isochemically, except for the introduction of H_2O. They consist of two or three Ca-Al hydrosilicates together with albite, white mica, quartz, chlorite, sphene, hematite, and/or magnetite. Ca- and Na-amphiboles are characteristic of greenschists and blueschists respectively. Common Ca-Al index minerals for the various low-grade metamorphic facies include Ca-zeolites, lawsonite, prehnite, pumpellyite, and epidote. Andradite-

grossular garnet has also been recorded in low-T recrystallization and in geothermal systems (Coomb et al., 1977; Schiffman, pers. comm., 1983). Compositions and abbreviations of these phases are shown in Table I. Except for considerable substitution of FeO for MgO in amphibole, mica, and chlorite, and Fe_2O_3 for Al_2O_3 in most of the Ca-Al silicates, compositions of these phases can be modelled by the system NCMASH. With the assumption of quartz, albite, chlorite, and aqueous fluid present in excess, their compositions can be further simplified onto a ternary diagram Al_2O_3–CaO-MgO (+excess albite, quartz, and fluid) as shown in fig. 2.

Petrogenetic grid

In the present study, $P-T$ relations of Ca-zeolites (stilbite, heulandite, laumontite, and wairakite), prehnite, zoisite-epidote, lawsonite, pumpellyite, plagioclase, actinolite, hornblende, chlorite, and glaucophane were constructed for the model system. Fig. 1 summarizes $P-T$ relations compiled from available experimental data mainly on stabilities for their own bulk compositions together with geometrically derived equilibria. Forty-nine univariant lines (which are listed in Table II) and twelve invariant points are shown. Except for experimentally determined curves (solid, thick lines), the $P-T$ positions of other univariant lines and invariant points are estimated from natural parageneses. The resulting curves were bound together by means of Schreinemakers' rule. In some places, the relations are well constrained; in others they hinge heavily on calculated slopes and deduced data from natural parageneses. Considerable care was taken to make the grid internally consistent.

It is important to emphasize that most of the

Table I. Compositions and abbreviations of phases and facies used in this paper

Lm = Laumontite, $CaAl_2Si_4O_{12} \cdot 4H_2O$	Qz = Quartz, SiO_2
Hu = Heulandite, $CaAl_2Si_7O_{18} \cdot 6H_2O$	Cc = Calcite, $CaCO_3$
St = Stilbite, $CaAl_2Si_7O_{18} \cdot 7H_2O$	Ar = Aragonite, $CaCO_3$
Wr = Wairakite, $CaAl_2Si_4O_{12} \cdot 2H_2O$	Jd = Jadeite, $NaAlSi_2O_6$
Lw = Lawsonite, $CaAl_2Si_2O_7(OH)_2 \cdot H_2O$	Am = Analcime, $NaAlSi_2O_6 \cdot H_2O$
Pr = Prehnite, $Ca_2(Al,Fe)_2Si_3O_{10}(OH)_2$	Cz = Clinozoisite, $Ca_2Al_3Si_3O_{12}(OH)$
Ol = Oligoclase	An = Anorthite, $CaAl_2Si_2O_8$
Zo = Zoisite, $Ca_2Al_3Si_3O_{12}(OH)$	Ep = Epidote, $Ca_2(Al,Fe)_3Si_3O_{12}(OH)$
Ab = Albite, $NaAlSi_3O_8$	Pm = Pumpellyite, $Ca_4(Al,Fe)_5MgSi_6O_{21}(OH)_7$
Gr = Grossular, $Ca_3Al_2Si_3O_{12}$	And = Andradite, $Ca_3Fe_2Si_3O_{12}$
Mt = Magnetite, Fe_3O_4	Grd = Grandite, $Ca_3(Al,Fe)_2Si_3O_{12}$
Ht = Hematite, Fe_2O_3	Pl = Plagioclase, $(CaAl,NaSi)AlSi_2O_8)$
F = fluid	Tr = Tremolite, $Ca_2Mg_5Si_8O_{22}(OH)_2$
ZEO = Zeolite facies	Act = Actinolite, $Ca_2(Mg,Fe)_5Si_8O_{22}(OH)_2$
BS = Blueschist facies	Gl = Glaucophane, $Na_2(Mg,Fe)_3Al_2Si_8O_{22}(OH)_2$
GS = Greenschist facies	Hb = Hornblende, $NaCa_2(Mg,Fe,Al)_5Si_6Al_2O_{22}(OH)_2$
AM = Amphibolite facies	Chl = Chlorite, $(Fe,Mg)_{6-x}Al_x(Si_{4-x}Al_x)O_{10}(OH)_8$
PrA = Prehnite-actinolite facies	PP = Prehnite-pumpellyite facies
EA = Epidote-amphibolite facies	PA = Pumpellyite-actinolite facies
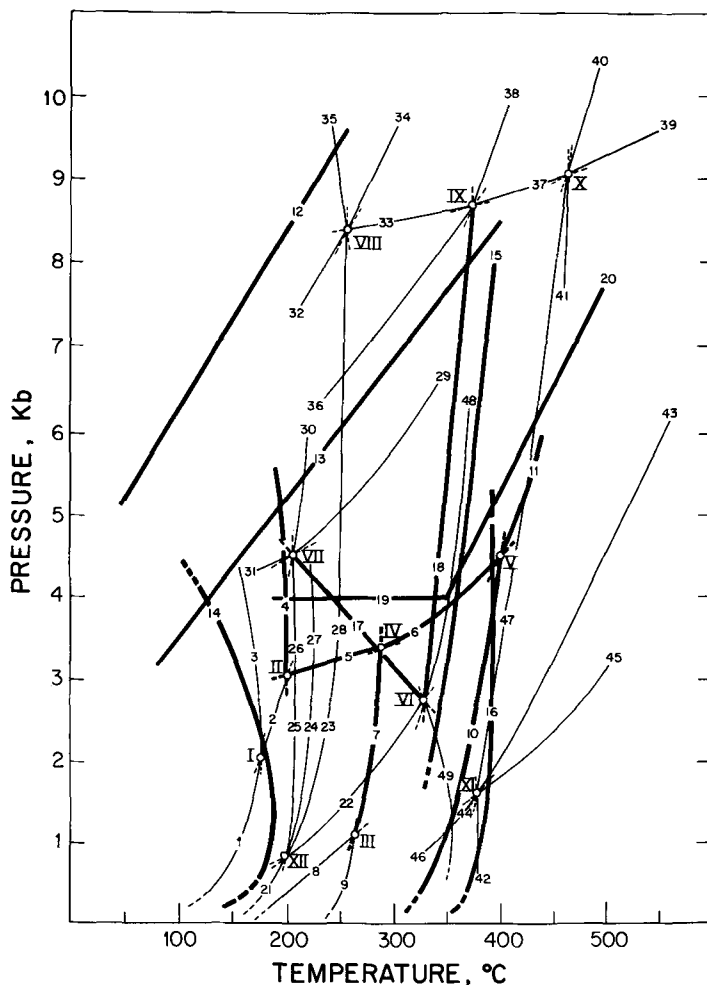
FIG. 1. P_{fluid}–T diagram for forty-nine univariant lines and twelve invariant points for the model basaltic system Na_2O–CaO–MgO–Al_2O_3–SiO_2–H_2O. Five univariant lines radiate from each of the invariant points VI–XII and three univariant lines radiate from each of the invariant points I to V. The forty-nine univariant reactions are listed in Table II and those experimentally determined reactions are shown as heavy lines.

reactions for the model system shown in fig. 1 are of the non-terminal type; thus they occur at lower temperatures than the thermal stability limit reactions for each phase alone. For example, the reaction (49) Pr + Chl + Qz = Zo + Tr + F defines a boundary between the prehnite-actinolite and greenschist facies; it occurs at lower temperatures than the maximum stability of prehnite defined by Pr = Gr + Zo + Qz + F determined by Liou (1971a). The upper temperature limit of the pumpellyite-actinolite facies for basaltic compositions is bounded by reaction (18) Pm + Chl + Qz = Cz + Tr + F which occurs at lower temperatures than the pumpellyite stability limit of Schiffman and Liou

(1980). Similarly, the blueschist-greenschist transition is defined by reaction (37) Gl + Zo + Qz + F = Tr + Chl + Ab which is different from the stability limits of glaucophane as determined by Carman and Gilbert (1983) and Maresch (1977).

Most workers have hypothesized that the pumpellyite-actinolite facies should have a minimum pressure limit, and its P-T field is commonly depicted as wedged-shaped, with an increasing temperature range at increasing pressures. The configuration of Nitsch's (1971) pumpellyite-forming and pumpellyite-consuming reactions has generally propagated this view; Nitsch's experimental study, therefore, is widely cited (Ernst, 1977,

Table II.   Univariant reactions for the model basaltic system (CANMSH) in low-
temperature metamorphism (P-T relations of these reactions are shown
in figs. 1 and 2). For phase compositions and abbreviations see Table I.

Reaction No.	Reaction	Reaction No.	Reaction
1.	St = Lm + F	2.	Hu = Lm + Qz + F
3.	St + Hu + F	4.	Hu = Lw + Qz + F
5.	Lm = Lw + Qz + F	6.	Lw + Qz = Wr + F
7.	Lm = Wr + F	8.	Lm + Qz = Yu
9.	Yu = Wr + Qz + F	10.	Wr = An + Qz + F
11.	Lw = An + Qz + F	12.	Jd + Qz = Ab
13.	Ar = Cc	14.	Am + Qz = Ab + F
15.	Pm = Zo + Gr + Chl + Qz + F	16.	Pr = Zo + Gr + Qz + F
17A.	Pr + Chl $(Mg_5 Al_2 Si_3 O_{10} (OH)_8)$+ F = Pm + Tr + Qz		
B.	Pr + Chl $(Mg_6 Si_4 O_{10} (OH)_8)$+ Qz = Pm + Tr + F		
19 & 20.	Stability limits of glaucophane (Maresch, 1977)		
18.	Pm + Chl + Qz = Zo + Tr + F	21 & 24.	Lm + Pr = Zo + Qz + F
22.	Pm + Qz = Zo + Pr + Chl + F	23.	Lm + Pm = Zo + Chl + Qz + F
25.	Pr + Chl + Lm = Pm + Qz + F	26.	Pr + Chl + Lw = Pm + Qz + F
27.	Pr + Lw + Qz = Zo + F	28.	Lw + Pm = Zo + Chl + Qz + F
29.	Pm + Chl + Qz + F = Lw + Tr	30.	Lw + Pr + F = Chl = Pm + Qz + F
31.	Lw + Tr = Pr + Chl + Qz + F	32.	Lw + Gl = Pm + Chl + Ab + Qz + F
33.	Pm + Chl + Ab = Zo + Gl + F	34.	Lw + Gl = Zo + Chl + Ab + Qz + F
35.	Lw + Pm + Ab = Zo + Gl + Qz + F	36.	Pm + Gl + Qz + F = Tr + Chl + Ab
37.	Zo + Gl + Qz + F = Tr + Chl + Ab	38.	Pm + Gl + Qz = Zo + Tr + Ab + F
39.	Zo + Gl + Qz + F = Hb + Chl + Ab	40.	Zo + Gl + Tr + Qz = Hb + Ab + F
41.	Tr + Chl + Ab = Hb + Gl + F	42.	Ol + Tr + Chl = Hb + Ab + F
43.	Zo + Chl + Ab + Qz = Ol + Hb + F	44.	Zo + Chl + Ab + Qz = Ol + Tr + F
45.	Zo + Hb + Ab + Qz = Ol + Tr + F	46.	Zo + Chl + Qz = Wr + Tr + F
47.	Zo + Chl + Tr + Qz = Hb + F	48.	Pm + Qz = Zo + Pr + Tr + F
49.	Pr + Chl + Qz = Zo + Tr + F		

1983). However, Schiffman and Liou (1980) suggested that the prehnite-consuming reaction to form pumpellyite + actinolite is different from that determined by Nitsch (1971) and the prehnite + chlorite assemblage should occur at higher temperature than the pumpellyite-actinolite assemblage. Therefore, there is no experimental or theoretical ground for invoking a minimum pressure limit for the pumpellyite-actinolite assemblage. Such a discrepancy is due to the choice of chlorite composition. Schiffman and Liou (1980) used a most aluminous chlorite to balance the reaction, 4 Mg–Al pumpellyite + 2 quartz = 8 prehnite + chlorite + $2H_2O$. Alternatively if Al-rich chlorite $(Mg_5Al_2Si_3O_{10}(OH)_8)$ and Mg end-member septechlorite $(Mg_6Si_4O_{10}(OH)_8)$ is used to relate the prehnite-pumpellyite and pumpellyite-actinolite facies, two reactions could be written:

A. Al-rich chlorite:
   20 pumpellyite + 3 tremolite + 6 quartz = 43 prehnite + 7 chlorite + $2H_2O$.
B. Mg-end chlorite:
   60 prehnite + 7 chlorite + 4 quartz = 24 pumpellyite + 12 tremolite + $20H_2O$.
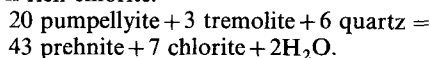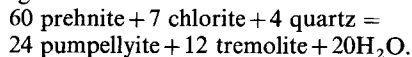
Therefore, depending on the choice of the chlorite composition, the prehnite-bearing assemblage could be stable at higher temperature (case A) or lower temperature (case B) than the pumpellyite-bearing assemblage.

Fig. 2 summarizes the key reactions defining facies boundaries for various low-grade metamorphic facies and their stable mineral assemblages for basaltic compositions. Although there is some uncertainty on *P-T* positions for some of the inferred reactions, it should be useful in designing further experiments and in determining mineral parageneses for various metamorphic facies series. In order to make the petrogenetic grid as complete as possible for low-grade metamorphism, stabilities of jadeite + quartz, calcite-aragonite and analcime + quartz are also included in figs. 1 and 2.

The new experimental results

P-T relations of some key reactions defining facies transitions were experimentally determined for the model basaltic system. Details for the experimental results will be described elsewhere (Maruyama *et al.*, in press). Preliminary results, summarized in fig. 3, include:

(2) heulandite = laumontite + quartz + H_2O, subdividing the zeolite facies;

(23) laumontite + pumpellyite = clinozoisite + chlorite + quartz + H_2O, marking the zeolite to prehnite-pumpellyite facies transition;

(17) prehnite + chlorite + quartz = pumpellyite + tremolite + H_2O, marking the prehnite-pumpellyite to pumpellyite-actinolite facies transition;
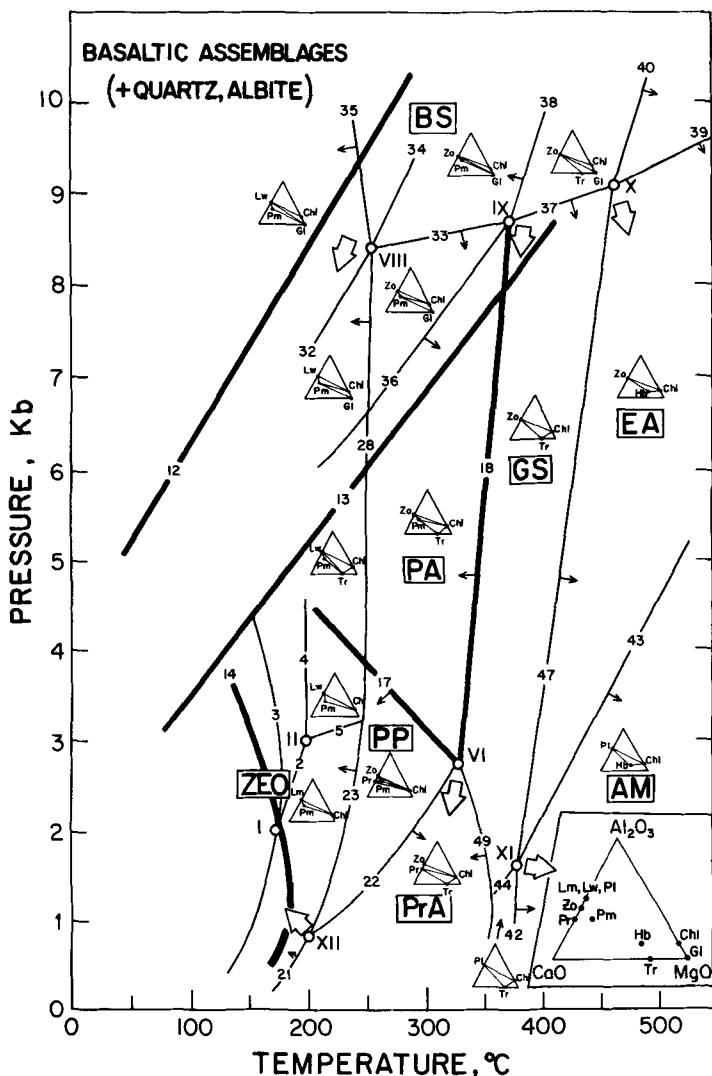
FIG. 2. P_{fluid}-T diagram showing a petrogenetic grid for various low-grade metamorphic facies (letters in boxes, see Table I for abbreviations) and their basaltic assemblages (+chlorite+quartz+albite) in the model basaltic system. Displacements of reaction curves and invariant points due to the introduction of Fe_2O_3 into the model system are shown by arrows (smaller arrows for univariant lines and larger arrows for invariant points).

(49) prehnite + chlorite + quartz =
   clinozoisite + tremolite + H_2O,
marking the prehnite-actinolite to greenschist facies transition;

(18) pumpellyite + chlorite + quartz =
   clinozoisite + tremolite + H_2O,
marking the pumpellyite-actinolite to greenschist facies transition; and

(37) glaucophane + clinozoisite + quartz +
   H_2O = chlorite + tremolite + albite,

marking the blueschist to greenschist facies transition.

Except for reaction (17), where the P-T slope is very sensitive to chlorite composition as described in previous sections, other reactions are well bracketed. In principle, reactions (17), (49), and (18) should define an invariant point VI as shown in fig. 2. However, because of uncertainties involved in experimental determination of these reactions and insufficient data and sensitivity of chlorite

composition for reaction (17), the curves shown in fig. 3 are not geometrically consistent. Therefore, for the subsequent discussion of phase relations among the prehnite–pumpellyite, prehnite–actinolite, and greenschist facies assemblages, P–T location of the invariant point VI is assumed to be at the intersection of the P–T curves for reactions (49) and (18).
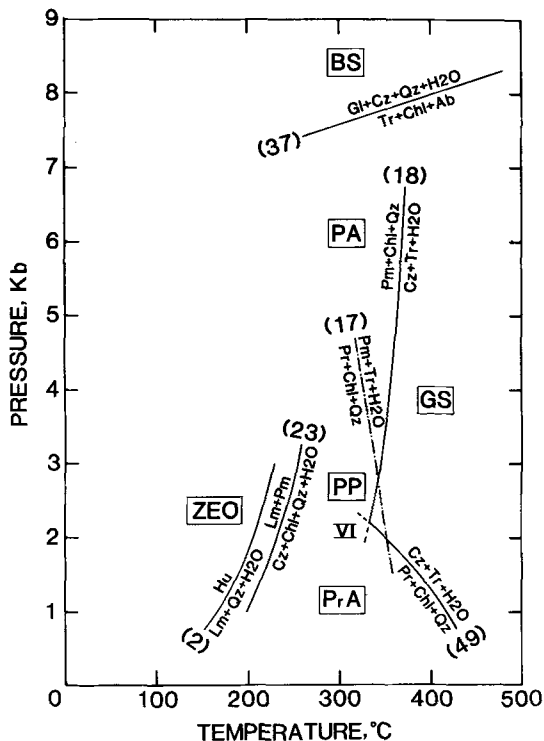
FIG. 3. P_{fluid}–T diagram showing six reactions which were experimentally determined in the present study for the model system. (See Table I for mineral abbreviations). The invariant point VI is located, and appropriate fields for the zeolite, prehnite–pumpellyite, prehnite–actinolite, pumpellyite–actinolite, blueschist and greenschist facies are shown.

The transition between the pumpellyite–actinolite and greenschist facies is defined by reaction (18) pumpellyite + chlorite + quartz = tremolite + epidote + H_2O. This reaction has been investigated by Nitsch (1971) using natural Fe-bearing phases but without controlling oxygen fugacity. Our result shown in fig. 3 is consistent with that of Nitsch and is about 20 °C lower than the maximum stability of pumpellyite determined by Schiffman and Liou (1980, reaction 15 of fig. 1).

Phase relations among greenschist, amphibolite, actinolite–plagioclase, and epidote–amphibolite facies have been described in detail elsewhere (e.g. Apted and Liou, 1983; Maruyama *et al.*, 1983). The following discussions focus on metabasaltic assemblages for the zeolite, prehnite–pumpellyite, pumpellyite–actinolite, and blueschist facies. One must be fully aware that every facies boundary in the diagram is essentially a transition zone in nature, because of FeO or Fe_2O_3 in the participating phases and variation in fluid composition. Moreover, many facies boundaries are defined by continuous reactions in which both compositions and proportions of the reacting phases vary in P–T space.

The Al–Ca–Fe^{3+} projection

The phase relations shown in figs. 1 and 2 are for the model basaltic system without FeO and Fe_2O_3. With the introduction of these components, the ratios Fe_2O_3/Al_2O_3 and FeO/MgO in reacting phases cause displacements of the facies boundaries. The shifts of some univariant lines and invariant points are qualitatively shown by arrows in fig. 2 and quantitatively contoured by isopleths of epidote composition in terms of $X_{Fe^{3+}}$ around the invariant points XII and VI in fig. 4. For example, on the introduction of Fe^{3+} into the model system, reactions (49) and (18) around invariant point VI become continuous reactions and the invariant point becomes a discontinuous reaction. The P–T locations of the discontinuous reactions for $Lm + Pm + Qz = Pr + Ep + Chl + F$ (XII) and for $Pm + Qz = Ep + Pr + Tr + Chl + F$ (VI) are shown as heavy lines in fig. 4. At a given P and T condition, the participating phases defining a discontinuous reaction are fixed in composition. On the other hand, those assemblages defining continuous reactions have one more degree of freedom and may vary their compositions systematically with increasing temperature at constant pressure. Compositions of minerals in the assemblages defining either continuous or discontinuous reactions vary systematically with P and T, hence they constitute low-variance *buffered assemblages*. The composition of minerals for other than buffered assemblages may vary depending on the mineral assemblage and bulk composition. Such P–T–X relationships will be described in a later section. A similar treatment of the effect of Fe on the greenschist–amphibolite transition equilibria is described by Maruyama *et al.* (1983).

In order to evaluate such an effect on compositions of the coexisting phases in low-grade metabasites, a simplified 4-component projection Al–Ca–Fe^{3+}–(Fe + Mg) was used. Compositions of the common low-grade minerals are plotted in this tetrahedron in fig. 5A. The ranges of solid solutions
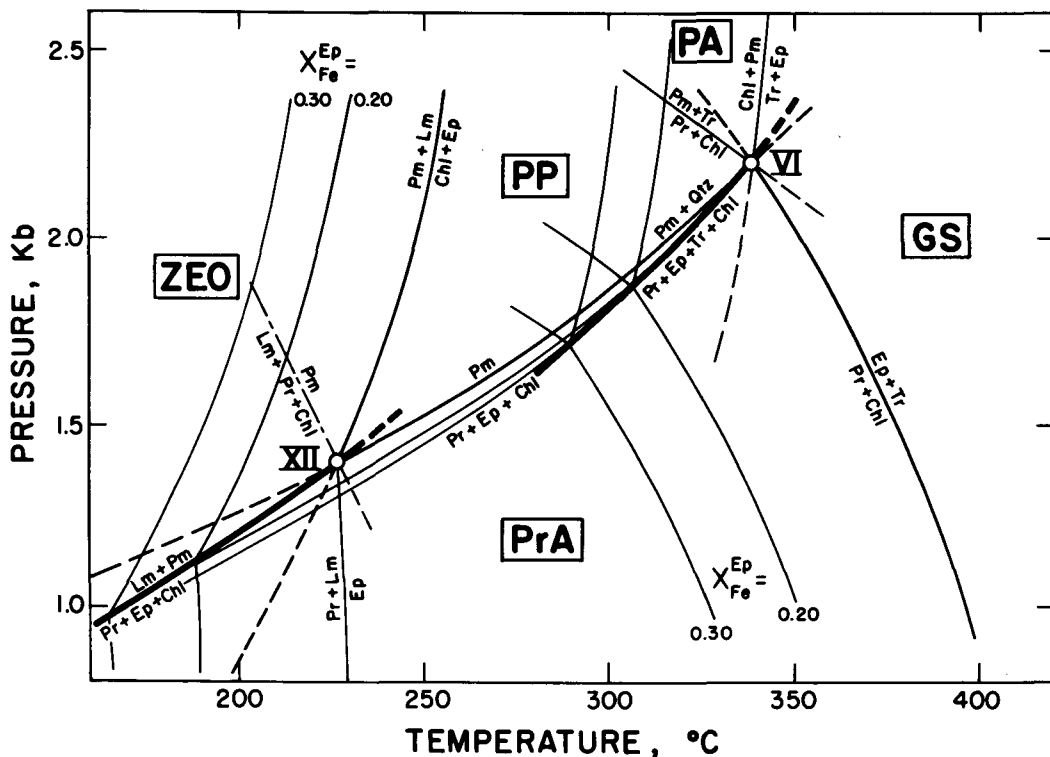
FIG. 4. $P_{fluid}-T$ diagram showing continuous reactions around the invariant points VI and XII and displacement of the invariant point along discontinuous reaction at the introduction of Fe_2O_3 into the model basaltic system. Series of isopleths were designated as X_{Fe} [= $Fe^{3+}/(Fe^{3+} + Al)$] of epidote for these continuous reactions. The $P-T$ location of the invariant point VI is from fig. 3 and that of the invariant point XII is estimated from combination of natural paragenesis with experimental data.

for epidote, prehnite, grandite garnet, pumpellyite, amphibole, and chlorite are shown. Other low-grade metamorphic minerals are either fixed in composition (e.g. laumontite, lawsonite, iron oxides) or present in excess (e.g. quartz, albite, sphene). If we restrict our discussion to subgreenschist facies assemblages, Ca-amphibole is confined to actinolite in composition and lies on the Ca–(Fe + Mg) join. The paragenetic relationships for blueschist facies assemblages are described elsewhere (Maruyama et al., in press).

The Al–Ca–Fe^{3+} plane was selected as the projection plane and chlorite of fixed composition as the projection point. This is justified by a number of factors: (1) variation of these minerals including pumpellyite is defined mainly by Fe^{3+}–Al substitution; (2) chlorite is ubiquitous in metabasite assemblages; and (3) compositions of these phases (except for amphibole) lie on or very close to the projection plane, hence a slight change in chlorite composition does not significantly affect their dispositions on the ternary diagram. Except for the Ca–Al silicates

which show significant solid solution (illustrated as solid lines), the other phases shown in the diagram have fixed compositions. Complete solid solution exists in the grandite garnet system. Liou et al. (1983) and Schiffman et al. (1984) suggest that epidote solid solution is continuous at least in the range of Ps 10 to Ps 33 and prehnite extends up to $X_{Fe^{3+}}$ = 0.30 without compositional discontinuity (see Liou et al., 1983, for discussion of compositional gaps for epidote and prehnite).

It should be pointed out that both hematite and magnetite were plotted at the Fe-apex. Depending on the oxidation state during metamorphism, hematite and/or magnetite occur in low-grade assemblages. The effect of f_{O_2} on compositional shifts for the projection has been discussed by Liou et al. (1983). Also shown in fig. 5B is the chemical composition of average basalt in terms of Al–Ca–Fe^{3+}–(Fe^{2+} + Mg); it lies very close to that of Al-pumpellyite. This diagram has been used by Coombs et al. (1977) to discuss variations in compositions and assemblages of andradite- and
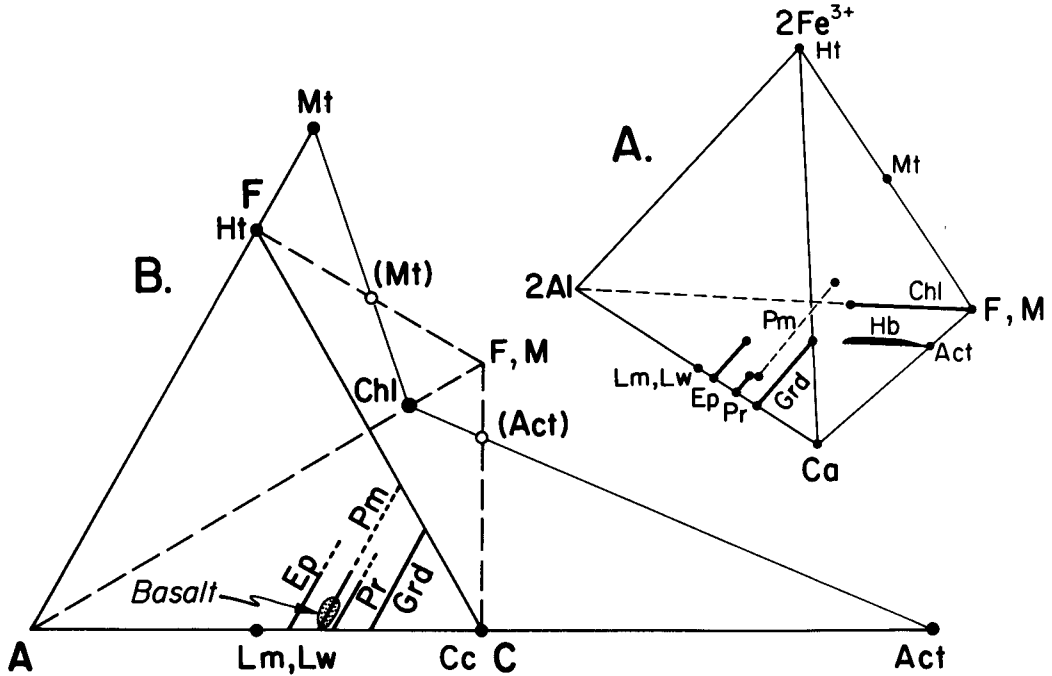
FIG. 5. A. Compositions of laumontite, lawsonite, epidote, prehnite, pumpellyite, grandite garnet, chlorite, actinolite, hornblende, and iron oxide in a tetrehedron $2Al-Ca-2Fe^{3+}-(Fe^{2+},Mg)$. Compositional ranges of these phases are shown. B. Projection of these phases from a chlorite composition on to a $2Al-Ca-2Fe^{3+}$ diagram. Note that the compositional variations of prehnite, epidote, pumpellyite, and grandite garnet are parallel to each other. Basaltic compositions are also shown.

grandite-bearing assemblages in low-grade metamorphic rocks from New Zealand. Some of their data are incorporated in fig. 6 for the present discussion.

Mineral paragenesis in low-grade metamorphism

The paragenetic sequences of various low-grade metamorphic facies series are plotted in fig. 6. The diagram shows (*a*) observed mineral assemblages (+quartz, albite, chlorite), (*b*) analysed mineral compositions, and (*c*) continuous and discontinuous reactions in progressive metamorphism of basaltic rocks as related to low-, intermediate-, and high-pressure facies series. Compositions and assemblages of metabasaltic minerals are plotted for the Karmutsen basalts (fig. 6A to G; Kuniyoshi and Liou, 1976*a*, *b*; Schiffman, 1978), for the East Taiwan ophiolite (fig. 6A and B; Liou, 1979; Ernst and Liou, in press), for the Del Puerto ophiolite fig. 6A to D; Evarts and Schiffman, 1983), for New Zealand metabasites (fig. 6A to D and H to J; Kawachi, 1975; Coombs *et al.*, 1977; Houghton, 1982), and for Sanbagawa metabasites (fig. 6K to M;

Nakajima *et al.*, 1977). Results of recent study on burial metamorphic sequence in Chile (Levi *et al.*, 1982) and in Western Australia (Smith *et al.*, 1982) were also used.

Coexistence of two or three Ca–Al silicates together with magnetite (or hematite or pyrite), chlorite, albite, and quartz from various localities are listed in Table III. Although equilibrium is difficult to demonstrate for low-grade mineral assemblages, the systematic and predictable changes in mineral parageneses and compositions with increasing grade indicate that equilibrium has been approached sufficiently closely such that stable mineral assemblages can be identified. Reactions for facies boundaries and index mineral assemblages for various low-grade metamorphic facies are briefly described below.

Zeolite facies. The zeolite facies defined by Coombs *et al.* (1959, p. 91) includes '. . . at least all those assemblages produced under physical conditions in which the following are commonly formed: quartz–analcime, quartz–heulandite, and quartz–laumontite'. The critical mineral assemblages are analcime–heulandite–quartz–chlorite

$$Fe^{3+} - Pm = And + Ht (Mt) + Chl + H_2O$$

$$Al - Pm = Zo + Pr + Chl + H_2O$$
$$Chl + And = Ht + Act + H_2O \qquad Chl + Pr + Ht = Ep + Act + H_2O$$

$$And + Chl = Ht + Act + H_2O$$

NEW ZEALAND

$$Fe^{3+} - Pum + Ht = Ep + Act + Chl + H_2O$$
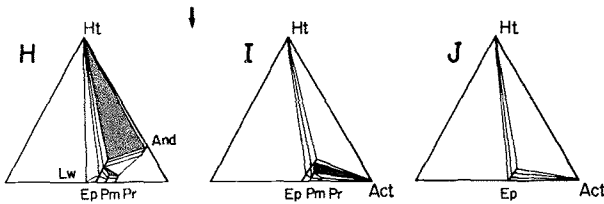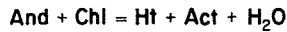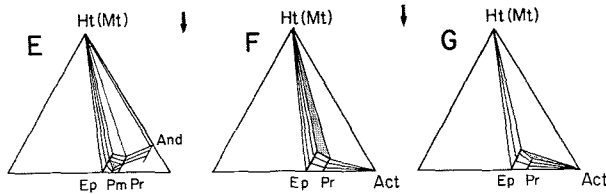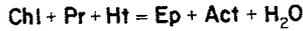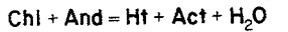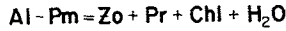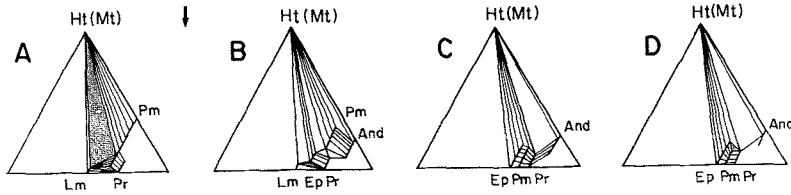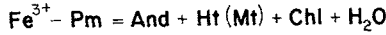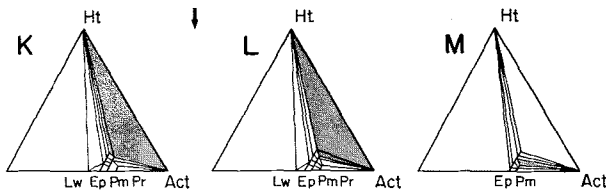
SANBAGAWA

FIG. 6. Series of isobaric $2Al-Ca-2Fe^{3+}$ diagrams showing recognized (shaded) and inferred 3-phase and 2-phase assemblages $(+Qz+Chl+Ab)$ in sub-greenschist facies metabasites including those from New Zealand and Sanbagawa, Japan (see Table III for data source and mineral assemblages). These diagrams are expected to be modified with new information. For instance, our recent data on the Karmutsen metabasites (Cho *et al.*, in press) suggest a few more parageneses between those shown in A, B, and C.

and laumontite–albite–quartz–chlorite ($\pm$ pumpellyite). The subdivision of the facies probably occurs at a temperature around 180 °C where analcime + quartz give way to albite, and heulandite decomposes to laumontite + quartz.

Mineral assemblages for zeolite facies metabasites are shown on fig. 6A and B. Assemblages laumontite + Fe-pumpellyite + hematite,   Lm + Pm + Pr and Lm + Pr + Ep have been identified. Preliminary data on the compositions of these

Table III. Reported occurrences of 3-phase assemblages (+chlorite+albite+quartz) in low-grade
metamorphic rocks

Diagram	Mineral assemblage	Locality & Reference
	I. Zeolite facies	
A	Lm – Pm – Ht	East Taiwan Ophiolite (Liou, 1979)
		Del Puerto Ophiolite, CA (Evarts and Schiffman, 1983)
		Takitimu, N. Z. (Houghton, 1982)
	Lm – Pm – Pr	Del Puerto Ophiolite, CA (Evarts and Schiffman, 1983)
		Takitimu, N. Z. (Houghton, 1982)
		Central Chile (Levi et al., 1982)
B	Lm – Ep – Pr	Onikobe geothermal system (Liou et al., in press)
	And – Pm – Ht	Takitimu, N.Z. (Houghton, 1982)
	Grd – Pr – Pm	Takitimu, N.Z. (Houghton, 1982)
	II. Prehnite–pumpellyite facies	
C	And – Pr – Ht	New Zealand (Coombs et al., 1977)
	Pr – Pm – Ht	Del Puerto Ophiolite (Evarts and Schiffman, 1983)
D,E	Pr – Pm – Ep	Del Puerto Ophiolite (Evarts and Schiffman, 1983)
		Karmutsen volcanics (Kuniyoshi and Liou,
		1976; Cho et al., in prep.)
		Takitimu, N.Z. (Houghton, 1982)
	III. Prehnite–actinolite facies	
F	Ep – Pr – Ht	Del Puerto Ophiolite (Evarts and Schiffman, 1983)
	Ep – Pr – Mt	Cerro Prieto geothermal (Bird et al., 1984)
		Karmutsen Volcanics (Kuniyoshi and Liou, 1976)
G	Ep – Pr – Act	Karmutsen volcanics (Kuniyoshi and Liou, 1976)
		Tanzawa Mtn. (Seki et al., 1969)
		Del Puerto Ophiolite (Evarts and Schiffman, 1983)
		Cerro Prieto geothermal (Bird et al., 1984)
	IV. Lawsonite–albite facies in N.Z. and Sanbagawa, Japan	
H	Lw – Ep – Pm	Wakatipu, N.Z. (Kawachi, 1975)
	Ep – Pr – Pm	
	And – Ep – Ht	N. Z. (Coombs et al., 1977)
	Grd – Ep – Pr	
K	Ep – Pm – Ht	Sanbagawa (Nakajima et al., 1977)
	Pm – Act– Ht	
	V. Pumpellyite–actinolite facies in N.Z. and Sanbagawa, Japan	
I,L,M	Ep – Pm – Act	Wakatipu, N.Z. (Kawachi, 1975)
		Sanbagawa (Nakajima et al., 1977)
L	Pm – Act – Ht	Sanbagawa (Nakajima et al., 1977)

phases from the Karmutsen metabasites indicate that both epidote and pumpellyite of the Lm + Pm + Ep assemblages increase their Al contents with increasing grade. Comparison of the disposition of minerals in fig. 6B and C results in a reaction Lm + Pm = Zo + Chl + H_2O, which defines the upper temperature limit of the zeolite facies. The maximum pressure under which zeolite assemblages are stable is probably around 3 kbar. At pressures greater than 3 kbar, lawsonite-bearing and prehnite–pumpellyite assemblages would dominate.

Prehnite–pumpellyite facies. Coombs (1960) and Seki (1961) proposed the prehnite–pumpellyite facies to fill the gap between the zeolite facies and the greenschist facies. Characteristic basaltic assemblages of this facies include pumpellyite–prehnite–chlorite; pumpellyite–chlorite–epidote; prehnite–pumpellyite–hematite (fig. 6C), and pumpellyite–prehnite–epidote (fig. 6D), together with other excess phases. In New Zealand, andradite–prehnite–hematite (fig. 6C) has been described by Coombs *et al.* (1977). Reaction 22, Pm + Qz = Zo + Pr + Chl + H_2O, defines the disappearance of pumpellyite and divides the *P–T* fields for the prehnite–pumpellyite and prehnite–actinolite facies assemblages (see below).

Prehnite–actinolite facies. For a low-pressure facies series, metabasites are characterized by the disappearance of pumpellyite and appearance of actinolite at *P–T* conditions transitional from the prehnite–pumpellyite to greenschist facies. A *prehnite–actinolite facies* is proposed here to describe metabasite assemblages of prehnite + actinolite + epidote + chlorite + albite + sphene (+ quartz) (fig. 6G) which occur at such transition

zones. They have been described in thermal meta-morphic aureoles such as the Tanzawa Mountains (Seki et al., 1969), the Karmutsen volcanics (Kuni-yoshi and Liou, 1976a, b) and Takitimu, New Zealand (Houghton, 1982), and for ocean-floor metamorphism at the Del Puerto ophiolite (Evarts and Schiffman, 1983) and the East Taiwan ophiolite (Liou and Ernst, 1979). Other assemblages characteristic of this facies include epidote + prehnite, together with hematite or magnetite, in the Del Puerto ophiolite, or in the Cerro Prieto geothermal field (Bird et al., 1984). The upper-T limit of the prehnite–actinolite assemblage is delimited by a continuous reaction (49): prehnite + chlorite + quartz = clinozoisite + tremolite + H_2O.

Pumpellyite–actinolite facies. In many regionally metamorphosed terrains, pumpellyite commonly stably coexists with actinolite. The pumpellyite-actinolite-chlorite assemblage occurs in deeply buried volcanics of considerable thickness and has become an index assemblage for the pumpellyite-actinolite facies. Many previous descriptions of the field relations and mineral parageneses, chemistries, and textures (e.g. Bishop, 1972; Zen, 1974; Kawachi, 1975; Coombs et al., 1976) have indicated that the pumpellyite-actinolite facies occupies a P-T field intermediate between the prehnite–pumpellyite and greenschist facies; facies boundaries were dis-cussed in previous sections. The stable basaltic assemblages in New Zealand and Sanbagawa, Japan, are shown in fig. 6.

Blueschist facies. Deeply subducted rock sections display blueschist facies assemblages. A broad P-T field for the blueschist facies is shown in fig. 2. Three P-T fields are recognized and they are respectively characterized by the stabilities of the assemblages lawsonite-glaucophane ± chlorite ± pumpellyite; pumpellyite-glaucophane ± chlorite ± epidote and epidote-glaucophane ± chlorite ± actinolite. Clino-pyroxene is common but excluded for present discussion. Some coexisting Ca–Al silicates (+ hematite) in blueschists from both New Zealand and the Sanbagawa belt of Japan are shown in Table III and graphically illustrated in fig. 6. Aragonite and jadeitic to omphacitic pyroxene are commonly associated with these assemblages. This facies is bounded by Lw + Pm = Zo + Chl + Qz + H_2O (28) and Pm + Gl + Qz + H_2O = Tr + Chl + Ab (36) against the pumpellyite-actinolite facies. The boundary between the blueschist and green-schist facies in the model system is defined by the reaction: Zo + Gl + Qz + H_2O = Tr + Chl + Ab (37) which was experimentally determined to have a gentle P-T slope and occurs at pressure of about 7.5 kbar as shown in fig. 3. Graphic representation of blueschist-facies assemblages and the nature of sliding equilibria for the blueschist–greenschist

transition zone are discussed elsewhere (Maruyama et al., in press).

T-$X_{Fe^{3+}}$ diagrams: continuous vs. discontinuous reactions

For the model basaltic system described in previous sections, five univariant lines should radiate from an invariant point. Because of the ubiquitous occurrence of chlorite in metabasites, the chlorite-absent lines are not shown in figs. 2 and 4. With the introduction of Fe_2O_3 into the model system, univariant lines become continuous re-actions and an invariant point a univariant line. Mineral assemblages for both continuous and discontinuous reactions are buffered assemblages. The systematic P-T displacements of both uni-variant lines and invariant points are illustrated in fig. 4 as a series of isopleths designated as $X_{Fe^{3+}}$ in epidote. Such compositional variations for epidote, prehnite, and pumpellyite are further shown on the series of Al–Ca–Fe diagrams in fig. 6. At constant pressure, partitioning of the Fe^{3+} and Al among the three coexisting phases varies continuously along T-$X_{Fe^{3+}}$ loops as shown in fig. 7. Each mineral in the assemblage of a continuous reaction has its own compositional loop and its composition is highly dependent on the buffered assemblage in which the mineral is found. For the chlorite-excess system described in this paper, four continuous reactions intersect at one discontinuous reaction, where compositions of four phases (+ chlorite + albite + quartz + fluid) and temperature are fixed at constant pressure (see Thompson, 1976, for details).

Fig. 7 illustrates T-X relations for two discon-tinuous reactions respectively for transition of the zeolite to the prehnite–pumpellyite facies and for transition of the prehnite–pumpellyite to the prehnite–actinolite facies. The first discontinuous reaction Lm + Pm + Qz = Pr + Ep + Chl + F occurs at a temperature of 185 °C and pressure of 0.9 kbar and the second discontinuous reaction at about 340 °C and 1.75 kbar. Because of a lack of precise P-T data for those reactions in the model system and lack of appropriate thermodynamic data for the phases considered in the present study, it is difficult to predict the binary loops in the T-$X_{Fe^{3+}}$ diagram. The $X_{Fe^{3+}}$ values of prehnite, epidote, and pumpellyite employed in fig. 7 are from microprobe analyses of these phases in buf-fered assemblages in a progressive metamorphic sequence of the Karmutsen metabasites on Van-couver Island (Cho et al., in press). Preliminary data indicate that compositions of these phases vary systematically with increasing temperature. For example, both prehnite and epidote of the zeolite facies buffered assemblage Lm-Ep-Pr-Chl-Ab and
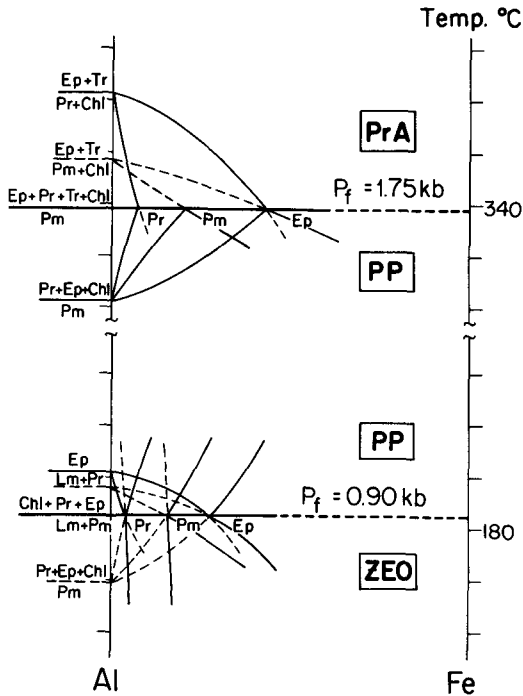
FIG. 7. Schematic isobaric $T-X_{Fe}$ diagrams showing compositional variations of buffered assemblages for continuous and discontinuous reactions. The bottom and top diagrams respectively illustrate the relationship for the zeolite and prehnite–pumpellyite facies transition and for the prehnite–pumpellyite and prehnite–actinolite facies transition. Temperature estimates and compositions of Ca–Al silicates are from Cho et al. (in press).

of the prehnite–actinolite facies buffered assemblage Ep–Pr–Act–Chl–Ab display increased Al contents with increasing temperature. On the other hand, prehnite, epidote, and pumpellyite of the prehnite–pumpellyite facies metabasites show decreased Al contents with increasing grade. Hence, compositional trends of these Ca–Al silicates in progressive sequences may become very complicated, depending on the rock bulk composition and mineral assemblage.

It should be pointed out that compositions of epidote, prehnite, and pumpellyite from non-buffered assemblages in the same Karmutsen metabasites were also analysed; they have a large compositional range and their variations are not systematic with grade. Previous suggestions on compositional trends for pumpellyite or epidote in metabasites are apparently oversimplified.

Fig. 7 exemplifies the complication of compositional variations of these Ca–Al silicates with increasing temperature. It was constructed from (1)

experimental data on the Al-end member reactions for the model basaltic system, (2) thermodynamic calculations on $T-X_{Fe^{3+}}$ loops, and (3) analysed compositions from the Karmutsen metabasites. Systematic experimental and compositional data are needed to complete such isobaric $T-X_{Fe^{3+}}$ relations. Nevertheless, such a diagram illustrates the following features: (1) both continuous and discontinuous reactions are easily recognized; (2) the Fe^{3+}-Al partitioning among the coexisting Ca–Al silicates for buffered assemblages can be quantitatively estimated and compositions of Ca–Al silicates are highly dependent on mineral assemblages; and (3) complex compositional trends for Ca–Al silicates in a low-T metamorphic sequence from the zeolite through prehnite–pumpellyite to prehnite–actinolite facies can be satisfactorily shown.

Summary

From an extensive literature review on the progress of low-temperature metamorphic studies (e.g. Seki and Liou, 1981; Liou, 1983) and systematic field and experimental investigations of metabasite assemblages in recent years (e.g. Liou et al., 1983; Cho et al., in press; Maruyama et al., in press), we conclude that the CNMASH system is best to model phase equilibria and mineral parageneses for low-temperature metamorphism of basaltic rocks. This system was further simplified with the assumption of excess albite, quartz, and chlorite of nearly constant composition in sub-greenschist facies metabasites. Compositions of common low-T metamorphic minerals are plotted in the Al_2O_3–CaO–MgO diagram and phase relations are defined by many invariant points from which three to five univariant lines radiate. Univariant reactions marking the transition of various low-temperature metamorphic facies were identified. Some of them were experimentally determined and a consistent petrogenetic grid was delineated for the model system. The stable $P-T$ conditions of these univariant reactions differ from those maximum stabilities of index minerals determined for their own bulk composition.

Application of such a petrogenetic grid for the model system to natural parageneses requires consideration of additional Fe_2O_3 and FeO components. Introduction of these additional components to the model system results in creation of sliding equilibria for boundaries of various low-T metamorphic facies and of discontinuous reactions for the invariant points of the model system. Examples of the continuous reactions around two invariant points for the transition from the zeolite through prehnite–pumpellyite to

prehnite-actinolite facies are illustrated. The $X_{Fe^{3+}}$ isopleths are quantitatively determined and the T-$X_{Fe^{3+}}$ relations were delineated from experimentally determined phase equilibria and from available thermodynamic and compositional data of epidote, prehnite, pumpellyite, and laumontite in the presence of quartz, albite, and chlorite. Compositions of these phases can be used to constrain the intensive properties for metamorphism only when they are from buffered assemblages. It is emphasized that composition of minerals from non-buffered assemblages should not be used to correlate with P and T and hence metamorphic grade.

In order to delineate the distribution coefficient for co-existing Ca-Al silicates in low-grade metabasites, an isobaric Al-Ca-Fe^{3+} plot from the chlorite projection is proposed. This diagram is best applied to low-T metamorphic rocks where two or three Ca-Al silicates occur. It (1) illustrates mineral assemblages and compositions of the co-existing Ca-Al silicates in the presence of quartz, albite, and chlorite at constant P and T, (2) delineates the compositional variations of buffered assemblages in terms of Fe^{3+}/Al ratio as a function of P and T, and (3) illustrates a series of discontinuous reactions with increasing grades. Reported occurrences of the Ca-Al silicates in the zeolite, prehnite-pumpellyite, pumpellyite-actinolite and prehnite-actinolite facies metabasites from classic burial metamorphic terrains and ocean-floor metamorphic rocks are presented in such a diagram.

It is apparent that the natural parageneses of low-T metamorphism are complicated: phase equilibria of the model system and partition coefficients among Ca-Al silicates in buffered assemblages must be known for success in delineation of a quantitative petrogenetic grid. Further experiments on sliding equilibria involving Ca-Al silicates and quantitative data of Fe^{3+}/Al partitioning from carefully documented metabasites are needed.

REFERENCES

Apted, M., and Liou, J. G. (1983) *Am. J. Sci.* **283**-A, 328–54.

Bird, D. K., Schiffman, P., Elders, W. A., and Williams, A. E. (1984) *Econ. Geol.* **79**, 671–95.

Bishop, D. G. (1972) *Geol. Soc. Am. Bull.* **83**, 3177–98.

Bowen, N. L. (1928) *The evolution of the Igneous Rocks.* Princeton Press, Princeton, New Jersey, 332 pp.

Carman, J. H., and Gilbert, M. C. (1983) *Am. J. Sci.* **283**-A, 414–37.

Cho, M., Liou, J. G., and Maruyama, S. (in press) *J. Petrol.*

Coombs, D. S. (1960) *21st Int. Geol. Congr. Copenhagen,* **13**, 339–51.

——Ellis, A. J., Fyfe, W. S., and Taylor, A. M. (1959) *Geochim. Cosmochim. Acta,* **17**, 53–107.

——Kawachi, Y., Houghton, B. F., Hyden, G., Pringle, I. J., and Williams, J. G. (1977) *Contrib. Mineral. Petrol.* **63**, 229–46.

——Nakamura, Y., and Vuagnat, M. (1976) *J. Petrol.* **17**, 440–71.

Ernst, W. G. (1977) *Rend. Soc. Ital. Mineral. Petrol.* **33**, 191–220.

——(1983) *Geol. Soc. China, Mem.* **5**, 229–68.

——and Liou, J. G. (in press) *Ofioliti.*

Evarts, R. C., and Schiffman, P. (1983) *Am. J. Sci.* **283**, 289–340.

Houghton, B. F. (1982) *N.Z. J. Geol. Geophys.* **25**, 1–19.

Kawachi, Y. (1975) Ibid. **18**, 401–41.

Kuniyoshi, S., and Liou, J. G. (1976a) *Am. J. Sci.* **276**, 1096–119.

——and Liou, J. G. (1976b) *J. Petrol.* **17**, 73–9.

Levi, B., Aguirre, L., and Nystrom, J. O. (1982) *Contrib. Mineral. Petrol.* **80**, 49–58.

Liou, J. G. (1971a) *J. Petrol.* **12**, 379–411.

——(1971b) *Am. Mineral.* **56**, 507–31.

——(1979) Ibid. **64**, 1–14.

——(1983) *Geol. Soc. China Mem.* **5**, 47–66.

——and Ernst, W. G. (1979) *Contrib. Mineral. Petrol.* **68**, 335–48.

——Kim, H. S., and Maruyama, S. (1983) *J. Petrol.* **24**, 321–42.

——Seki, Y., Guillemette, R., and Sakai, H. (1985) *Chem. Geol.* **49** (in press).

Maresch, W. V. (1977) *Tectonophysics,* **43**, 109–25.

Maruyama, S., Liou, J. G., and Cho, M. (in press).

——Suzuki, K., and Liou, J. G. (1983) *J. Petrol.* **24**, 583–604.

Nakajima, T., Banno, S., and Suzuki, T. (1977) *J. Petrol.* **18**, 263–84.

Nitsch, K. H. (1971) *Contrib. Mineral. Petrol.* **30**, 240–60.

Presnall, D. C., Dixon, J. R., O'Donnell, T. H., and Dixon, S. A. (1979) *J. Petrol.* **20**, 3–35.

Schiffman, P. (1978) Unpubl. Ph.D. thesis, Stanford University.

——Elders, W. A., Williams, A. E., McDowell, S. D., and Bird, D. K. (1984) *Geology,* **12**, 12–15.

——and Liou, J. G. (1980) *J. Petrol.* **21**, 441–74.

Seki, Y. (1961) *J. Petrol.* **2**, 407–23.

——and Liou, J. G. (1981) *Geol. Soc. China, Mem.* No. 4, 207–28.

——Oki, Y., Matsuda, T., Mikami, K., and Okumura, K. (1969) *J. Japan Ass. Mineral.* **61**, 1–75.

Smith, R. E., Perdrix, J. L., and Parks, T. C. (1982) *J. Petrol.* **23**, 75–102.

Thompson, A. B. (1976) *Am. J. Sci.* **276**, 401–24.

Zen, E.-A. (1974) *J. Petrol.* **15**, 197–242.